D_{5h}-(I)-C_{90}: between Fullerenes and Carbon Nanotubes

Óscar Jover Arrate

Máster en Nanociencia y Nanotecnología

MÁSTERES
DE LA UAM
2018 – 2019

Facultad de Ciencias

UAM Universidad Autónoma
de Madrid

excelencia UAM CSIC+

Master in

Nanoscience & Nanotechnology

D_{5h}-(I)-C_{90}: between Fullerenes and Carbon Nanotubes.

Óscar Jover Arrate

Director and tutor: Roberto Otero Martín

Laboratory: Institute IMDEA Nanoscience

FACULTAD DE CIENCIAS

Trabajo Fin de Máster. Curso 2018-2019

Universidad Autónoma de Madrid

Contents

1. Abstract

In this Master Thesis, we have investigated $D_{5h}(I)$-C_{90}, an isomer of C_{90}, a member of the fullerene family with the structure of a short capped nanotube, composed of 90 carbon atoms. In our experiments, we conducted Scanning Tunnelling Microscopy (STM) and Spectroscopy (STS) studies of the molecules deposited on noble metal substrates, Ag (111) and Au (111), as well as on ultra-thin NaCl layers. Topography images reveal that, when the molecules are deposited on these metals, the self-assembly is rhomboidal, with the long axis of the molecules parallel to the surface, maximizing the molecule-substrate interaction. However, when the molecules are deposited on a NaCl covered Ag (111) sample, they lie vertically on top of the NaCl patches, maximizing the lateral intermolecular interaction. This behaviour is similar to carbon nanotubes (CNT), that tend to aggregate laterally forming fibre bundles. We thus show that this isomer is an intermediate specie between fullerenes and CNT's and, by controlling the interaction between the molecules and the substrate, the character of the molecules may be changed from a CNT-like, to a fullerene-like behaviour. In addition, we investigate the energy level alignment and shape of the molecular orbitals (MO) of the C_{90} molecules by means of STS, lock-in maps, and Current Imaging Tunnelling Spectroscopy (CITS). We demonstrate that the energy differences between the MO's of the C_{90} molecules on Au (111) and on Ag (111), are a consequence of the different work functions of Au and Ag.

2. Introduction

Carbon is an element that, due to its valence, can form many allotropes. Some of these allotropes, such as diamond or graphite, have been known for a long time, and many more have been discovered in the previous decades. As some examples we mention, C_{60} also called buckminsterfullerene, graphene, nanotubes, nanobunds and nanoribbons. As the molecule of study in this Master Thesis, the isomer $D_{5h}(I)$-C_{90} shown in Figure 1b, presents an intermediate structure between fullerenes and CNT's, it can be expected to give relevant information about these species.

Fullerenes, are a kind of molecules formed by single and double bonds in order to create a closed or a partially closed mesh. The rings of these molecules are of five to seven atoms. They may present many different shapes such us hollow sphere, ellipsoid, tube.... The most famous fullerene is C_{60}, shown in Figure 1a, also known as "buckyball" as it resembles to the standard ball of association football.

They are typically named by their empirical formula C_n being n, the number of carbons of the molecule. Furthermore, for a given n, these molecules may present more than one isomer. Moreover, fullerenes have been intensively studied for their chemistry and technological applications in the fields of material science, electronics and nanotechnology [1]. Specially, they have been commonly used in the field of biomedicine. As some examples, we have the design of high-performance MRI contrast agents, X-ray imaging contrast agents, photodynamic therapy, drug and gene delivery [2] and acceptors on organic solar cells [3].

In the case of carbon nanotubes (CNTs), they are a type of nanostructure that consist of a two-dimensional hexagonal lattice of carbon atoms bent and joined in one direction forming a hollow cylinder (see Figure 1c). It is considered as an intermediate species between the closed shell type (buckyballs) and the flat sheet types (graphene). This allotropes of carbon naturally align themselves into bundles held together by Van der Waals forces.

Regarding their properties, their bond strength gives these molecules great mechanical stiffness and tensile strength. This unique strength is caused by orbital hybridization being the bonds between adjacent carbon atoms sp^2 orbitals, which are stronger than the sp^3 bonds in alkanes and diamond. CNT's also exhibit moderate chemical stability and high electrical and thermal conductivity [4]. These properties are well appreciated in many fields such as electronics, optics, composite materials, nanotechnology and materials science.

Due to the high cost of production, the applications of CNT's have been limited to the use of composite materials to improve their mechanical, thermal and electrical properties. However, it is estimated that by 2020 the cost will permit new applications [5], that are currently under development. As some examples we mention, the use of CNT's as a scaffold for diverse microfabrication techniques [6], energy dissipation in self-organized nanostructures under the influence of an electric field [1] and the use of CNT's for environmental monitoring due to their active surface and their ability to absorb gases [7].

Thus, the isomer $D_{5h}(I)$-C_{90} of the molecule C_{90}, as an intermediate specie between the previous ones will exhibit properties of fullerene or carbon nanotube. In order to observe this properties, we carried out the deposition of this isomer in three different

surfaces, two noble metals in which the molecule-substrate interaction is high, and NaCl covered Ag (111) in which we have a more electronically isolated environment from the substrate. In Figure 1, the stick and balls models of C_{60}, $D_{5h}(I)$-C_{90}, and a CNT is shown. From now on we will refer to $D_{5h}(I)$-C_{90} as simply C_{90}.
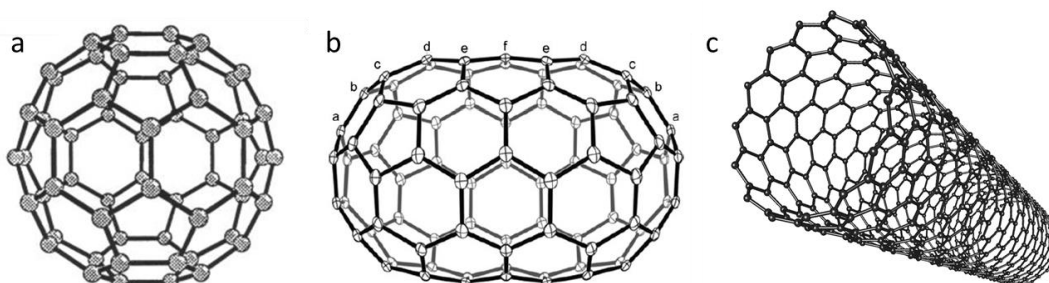

Figure 1: Stick and ball models of, a) C_{60}, b) C_{90} and c) CNT.

3. Experimental Methods

3.1. STM Principles

In order to study the self-assembly of the molecules on these three different substrates, we used Scanning Tunnelling Microscopy (STM). STM is a technique that gives the possibility of obtaining atomic resolution images of surfaces and molecules. In addition, it also permits atomic manipulation and spectroscopic studies on single molecules, atoms and surfaces. It was first developed by Gerd Binnig and Heinrich Rohrer at IBM Zürich in 1981, being awarded the Nobel prize in 1986 [8] [9].

In STM, images are obtained by placing a metallic tip over the substrate at a certain bias voltage between them and measuring the tunnelling current. The tunnelling current, is the flux of electrons that travels from the tip to the sample or vice versa (depending on the sign of the voltage) due to quantum tunnelling effect. Quantum tunnelling, is a quantum mechanical phenomenon in which a subatomic particle with energy E travels through a barrier potential of energy U_0 being $E < U_0$. Classically a particle of energy E cannot travel through a barrier potential of U_0 unless $E \geq U_0$. However, solving the Schrödinger stationary equation gives for a particle of energy $E < U_0$ and a potential barrier of length L a possibility of transmission of the particle. In Figure 2, the red line represents the probability to find the particle at a certain position. While this probability decreases exponentially through the classically forbidden region at the barrier, for narrow enough barriers it does not vanish, thus allowing for the transmission of the particle. [10]
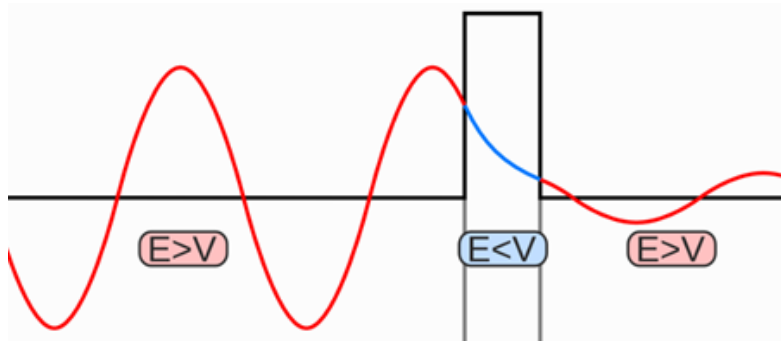
Figure 2: Quantum Tunnelling phenomenon. Although the barrier is higher in energy than the particle, there is a probability of transmission. [11]

As it was mentioned above, there are three basic elements on an STM which are represented in Figure 3. The metallic tip, with a certain sharpness, that can be positioned at a nanometric scale thanks to piezoelectric materials. [12] [13]. The sample, a metallic (or heavily doped semiconductor) surface in order to have electron transport. And the bias voltage between tip and sample. When it is zero, their Fermi levels align. However, when we apply a voltage, both Fermi levels are unbalanced. Thus there is an electron flux from the higher Fermi energy level to the lower level obtaining the so-called tunnelling current [8]. In Figure 4, it is represented the quantum tunnelling effect of the electrons that travel from the occupied states of the electrode with a higher Fermi level to the unoccupied states of the electrode with a lower Fermi level.
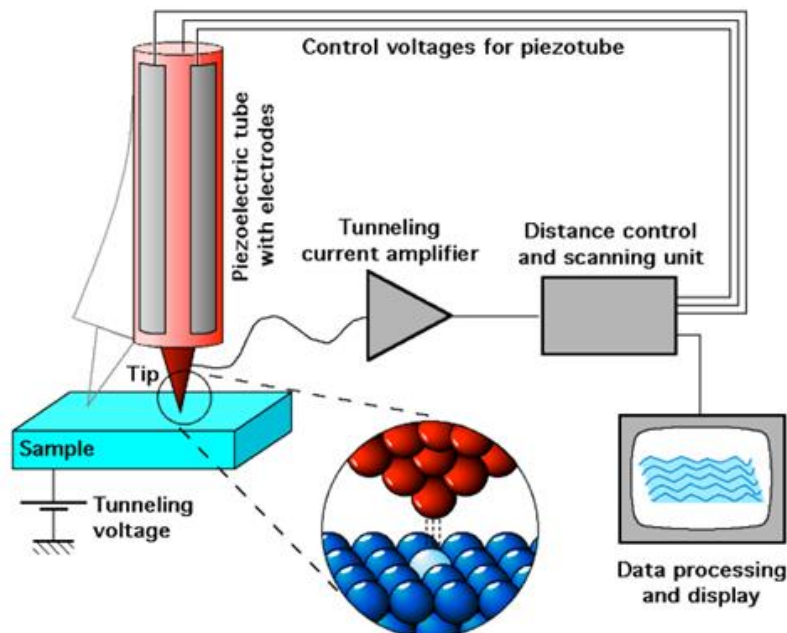

Figure 3: Schematic of the tip-sample system of the STM. The tip is controlled by a piezoelectric tube with electrodes and the tunnelling current is amplified before going to the data processor. [11]
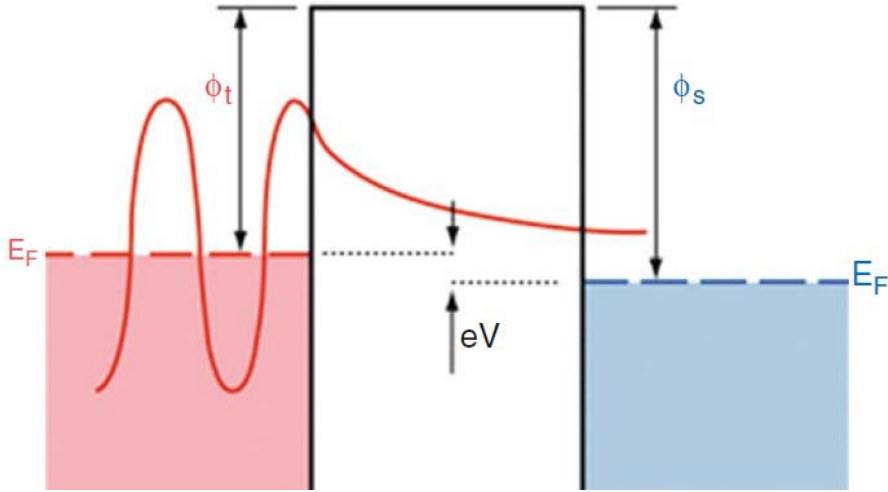
Figure 4: Schematic of the quantum tunnelling process taking place on an STM, the difference on the Fermi levels permits the tunnelling current. Subscript "t" refers to tip and "s" refers to the sample. [14]

The tunnelling current I is proportional to the tunnelling probability through the gap between the tip and the sample $\Im$ which is determined by the following expression[1] [13]:

$$\Im \propto \exp(-2z\sqrt{2m\phi/\hbar^2})$$

Being ϕ the work function, z the distance between the tip and the sample, m the mass of the electron and $\hbar^2$ the reduced Planck's constant. As the tunnelling current is a function of the bias voltage, it is possible to obtain spectroscopic information by taking the derivative of the current with respect to the voltage[2]. This derivative is proportional to the local density of states (LDOS) of the electrons of the orbitals of the substrate. [13]:

$$dI(V)/dV \propto \Im \sum_{j} \left| \psi_j(\mathbf{r_t}) \right|^2 \delta(\varepsilon_F + eV - \varepsilon_j)$$

There are two procedures of obtaining spectroscopic information with the STM:

▪ Lock-in maps: obtaining dI/dV images as a function of r_t at a fixed bias voltage and constant tunnelling current I_t.

▪ CITS or Current-Imaging Tunnelling Spectroscopy: obtaining dI/dV spectra at each point, this is equivalent to a set of lock-in maps for a given range of bias voltages. However, it gives much more information being consequently longer to acquire (approx. 15 hours). Usually, working at low Helium temperature is needed.

---

[1] The expression corresponds to the WKB approximation.
[2] This is done at zero temperature.

3.2. Experimental setup

The instrumentation for our experiments is located in one of the laboratories of the institute IMDEA nanoscience. In particular, the STM shown in Figure 5, is called photon-STM as it can let us study the local electronic induced light emission of the substrate. The experimental setup, is composed mainly of two different pumped chambers shown in Figure 6, the STM chamber where the measurements are taken and the preparation chamber, where molecular beam epitaxy processes on previously inserted single-crystals of noble metals takes place.

Before the molecular epitaxy growth process, we need the substrate to be clean and with terraces of hundreds of nanometres. This is done by sputtering, which is ionizing Ar atoms and accelerating them to collide with the surface of the single-crystal, and annealing, i.e. heating the sample with a Boron-nitride heater to flatten the sample. In order to keep the sample clean for long periods of time the base pressure on the chambers is Ultra High Vacuum ($\approx 10^{-10}$ mbar).

Once the sample is clean, the deposition of C_{90} and NaCl is done by an evaporator, where the molecules are placed on a glass crucible and heated until they reach their sublimating temperature, then, they adhere to the sample.
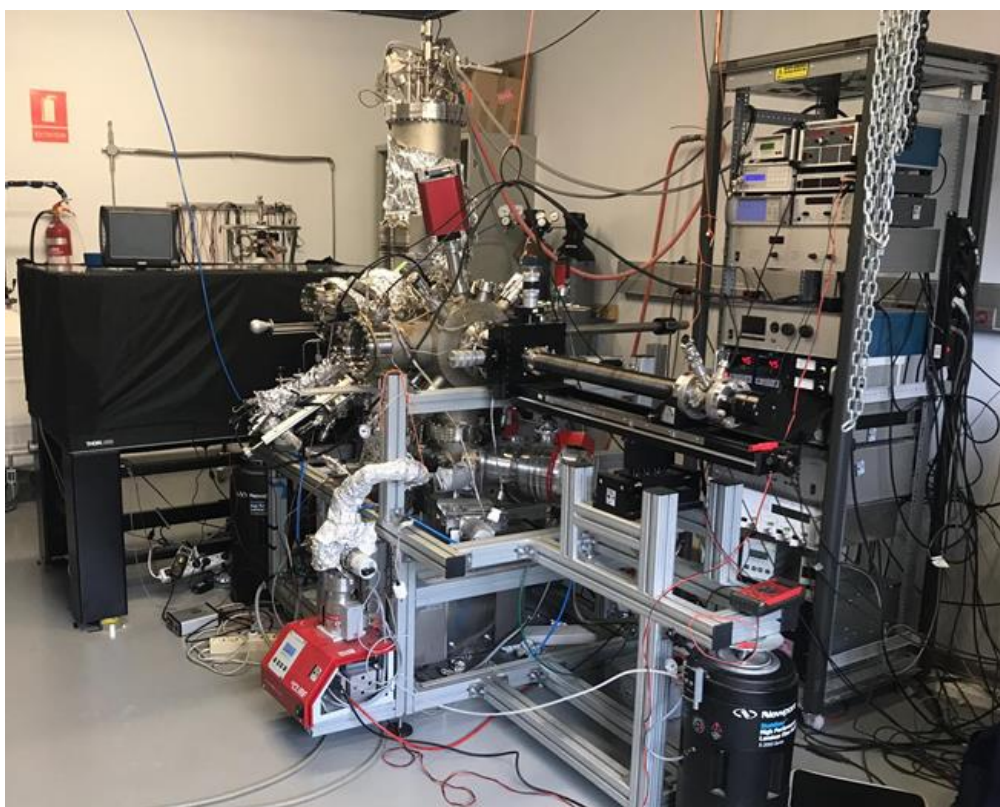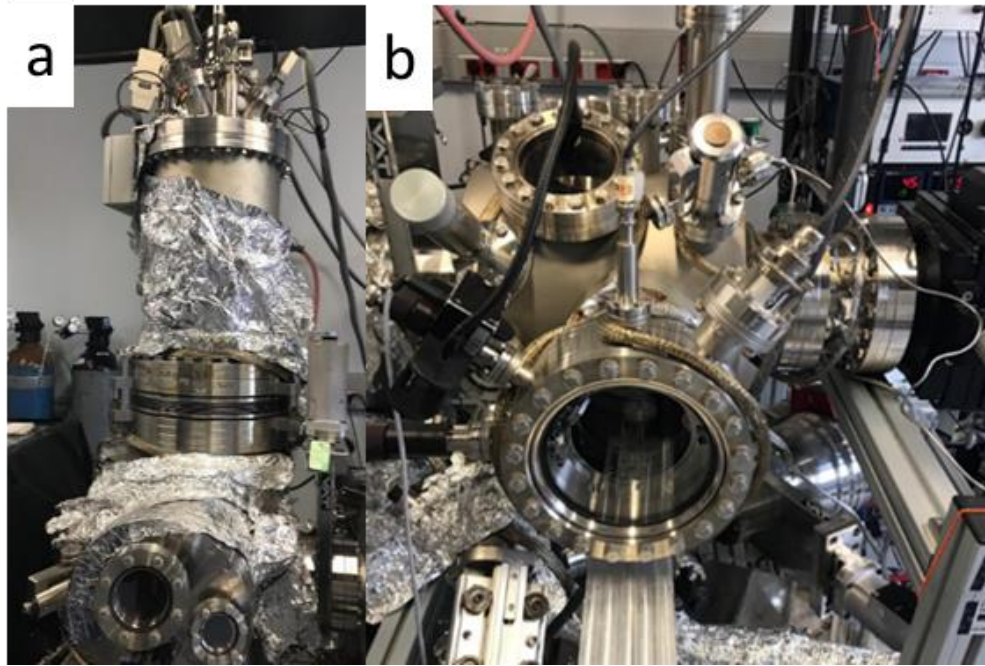

Figure 5: Image of experimental set-up.

9

Figure 6: a) The STM chamber, where the measurements are done. b) The preparation chamber, where the samples are produced.

One of the main problems that has to be taken into account when measuring with STM is that, as the tip moves in a range of nanometres, the minimization of vibrations is crucial, otherwise, there is the risk of crushing the tip. Thus, to minimize vibrations, the entire microscope is suspended over pneumatic platforms in a room that has its floor completely isolated from the rest of the building. Internally, the microscope is suspended by springs, and on its bottom, there are magnetic brakes that absorb the oscillations as it is shown in Figure 7.
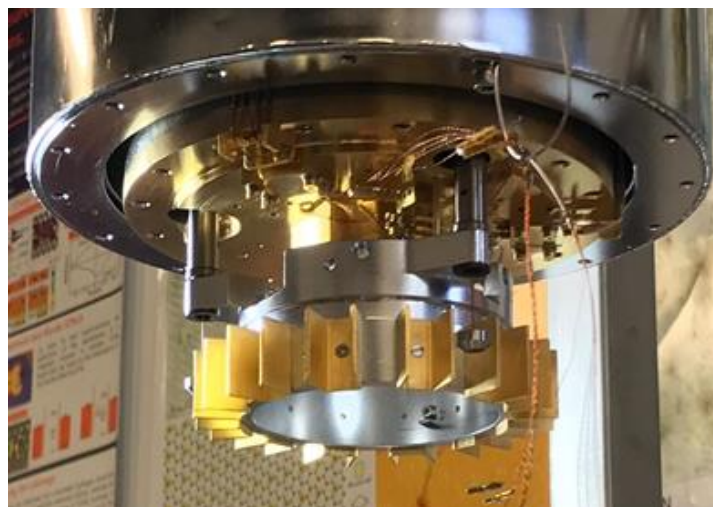
Figure 7: Backwards of the STM measurement instrumentation, the golden plates are the magnetic brakes that absorb vibrations.

4. Results

4.1. C$_{90}$ on Ag (111)

4.1.1. Self-assembly

The deposition of C$_{90}$ on Ag (111), was done at 480 ºC for 2 hours and after that, a post-annealing at 100 ºC for 10 minutes. At this conditions, it is shown in Figure 8a that the molecules nucleate on the steps of Ag (111) and a second layer forms on top of the first one. Thus, it was possible to study a bilayer of C$_{90}$. In Figure 8b, it is shown an island of C$_{90}$ where a small bilayer was formed. Moreover, we can also observe some differences in the brightness of the rows of the island. However, it is barely distinguishable until we reach, in Figure 8c, a small region with intermolecular resolution. Some columns appear brighter than others and although the origin of this observation is not yet clear it could be due to electronic or geometric effects.
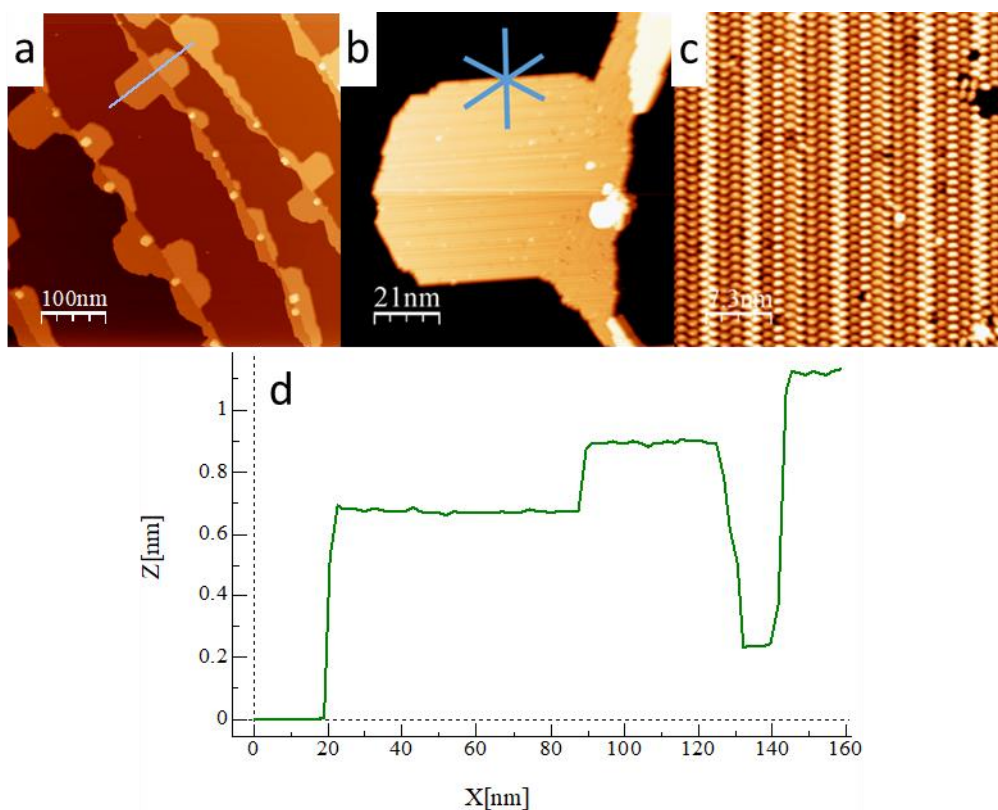

Figure 8: a) Islands of C$_{90}$ formed on the steps of Ag (111). b) An island of C$_{90}$ from image a. c) An intramolecular resolution image of the surface of the island. d) Height profile of an island of image a. Image information (Image size, bias voltage, tunnelling current) a) 500 x 500 nm; 2.50 V; 30.0 pA b) 107 x 107 nm; 2.50 V; 30.0 pA c) 36.5 x 36.5 nm; 1.10 V; 100.0 pA.

As it can be observed in Figure 8a the islands grow following the symmetry directions of the underlying substrate. In addition, as it is shown in Figure 8d, the height profile of the island reveals that its height is similar to the Van der Waals diameter of the molecule. In order to study the relation of these layers of C_{90} with respect to the substrate, it was necessary to take some measurements of the size of the molecules and its directions. Thus, in Table 1, there are presented all the relevant parameters of the size of C_{90} considering that the molecules present ellipsoidal shape. These data have been extracted from STM images like that on Figure 9, which shows an intermolecular resolution image of the molecules with the calculated parameters of its unit cell. This, and the data in Table 1 demonstrate that the molecules are adsorbed with the long axis parallel to the metal surface.
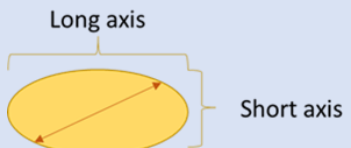
Measurement	Value (nm)	
Long axis distance	1.31 ± 0.04*	
Short axis distance	0.81 ± 0.02*	
Mean intermolecular diagonal distance (b_2)	1.345	
Mean intermolecular vertical distance (b_1)	0.975	

Table 1: Measurements of the most relevant distances of C_{90} in Ag (111). *Statistical values.
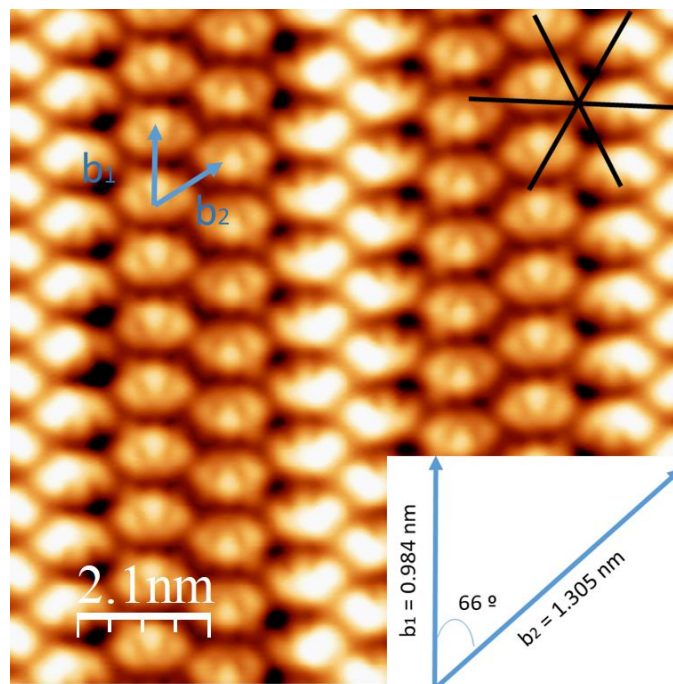
Figure 9: Intramolecular resolution image of C_{90} on Ag (111). Vectors b_1 and b_2 are the lattice vectors. The black star is the high symmetry directions of Ag (111). Image information (Image size, bias voltage, tunnelling current) 10.3 x 10.3 nm; 1.10 V; 1.0 nA.

With the information about the unit cell of the molecules and of Ag (111) we created a schematic representation of a C_{90} lattice over the substrate, shown in Figure 10. Considering b_1 and b_2 as the lattice vectors of C_{90} and a_1 and a_2 the lattice vectors of Ag (111) the relation between both groups of vectors is given by $b_1 = 4a_1 - 2a_2$; $b_2 = 2a_1 + 4a_2$. With this, we can conclude that the maximum interaction between C_{90} and Ag atoms makes this rhomboidal structure in which the molecules are placed with its long axis parallel to the surface and being the relation between its lattice vectors of integers.
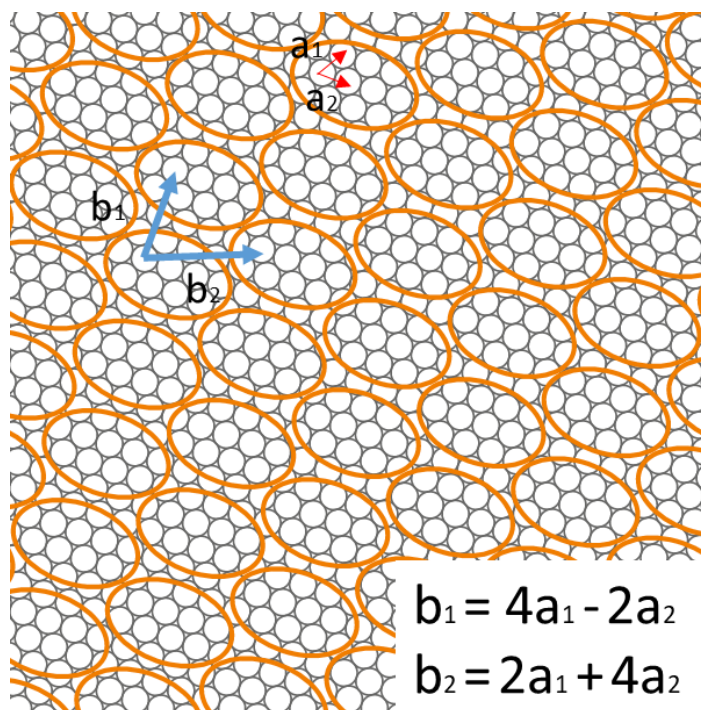

Figure 10: Schematic lattice of C_{90} on Ag (111) including the relation between the lattice vectors of the molecules (b_1, b_2) and the substrate (a_1, a_2).

Analysing a bilayer of C_{90} on Ag (111) presented in Figure 11a, we observed that the height profile shown in Figure 11b of the second layer is similar to the short axis distance of the molecules which tells us that they are also placed in a horizontal configuration. In order to maximize their interaction, the maximum area has to be in contact with the first layer. In Figure 11c, we also created a schematic lattice arrangement of the second

layer where it is seen that they are placed in the interstices of the first layer and following the same arrangement.
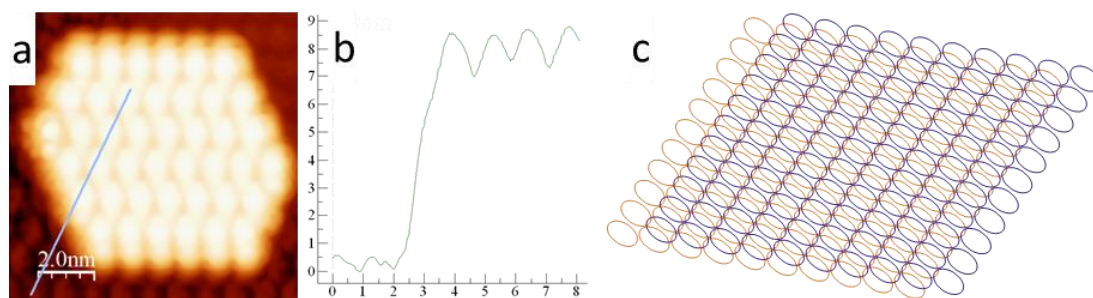

Figure 11: a) Topography image of a bilayer of C_{90}. b) Height profile of the bilayer. c) Schematic lattice of the bilayer of C_{90}. Image information (Image size, bias voltage, tunnelling current) a) 10.2 x 10.2 nm; 1.10 V; 30.0 pA.

4.1.2. Electronic structure

Figure 12 shows lock-in maps and topography images of the monolayer of C_{90}/Ag (111). The top row corresponds to topography images whereas the bottom row corresponds to dI/dV maps. As it was mentioned before, the second group gives information about the local density of states (LDOS) of the molecules. It has to be considered that on STM this LDOS images might also be influenced by the LDOS of the tip, but this effect has been discarded by comparison with spectroscopic measurements on the bare metal surface. The shape of the molecules in the topography images change for different bias voltages, having what it can be considered as "butterfly" shape from negative bias voltages until approximately 0.7 V. From 0.7 V to 1.5 V we observed that the shape of the molecule presents two big electronic lobes on both sides of the molecule and a small one in the middle. It is important to mention that the electronic cloud in the centre is sometimes in the upper part of some molecules and for others in the lower part. Finally, at 2.9 V the orbitals present an ellipsoidal shape. These changes can be traced back to the shape of the molecular orbitals by examining the dI/dV images. The observed molecular orbitals (MO's) of the molecules at different energies set by the bias voltage present different shapes: two electronic lobes at 0.065 V, a flower shape MO at 0.7 V, a circular lobe with a flatter lobe on top as the MO's shape at 1.5 V and a "doughnut" shape at 2.9 V.
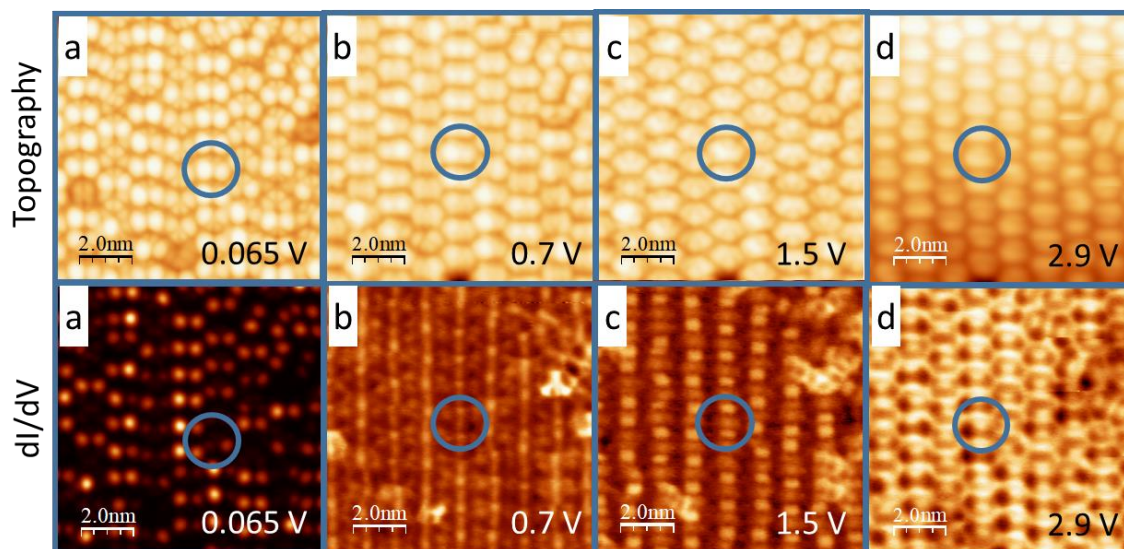
Figure 12: Topography and dI/dV images of the main molecular orbitals' shapes with respect to the bias voltages. Image information (Image size, tunnelling current) a) 10 x 10 nm; 150.0 pA b) 10 x 10 nm; 1.7 nA c) 10 x 10 nm; 2.5 nA d) 10 x 10 nm; 1.3 nA.

The identified MO's were further investigated by CITS. In Figure 13, a topography image is presented with three spectra in which we can observe some characteristic peaks at approximately -1.0 V, 0.0 V, 1.0 V and 2.5 V. Each of them corresponds to a different shape of the orbital having at -1.0 V the HOMO level and at 0.0 V another peak that corresponds to the LUMO level of C_{90}, for a better understanding, this peak is later compared to the spectra of C_{90} on Au (111). In Figure 14, there are also presented the dI/dV images of these peaks recorded by acquiring a CITS. Notice that the correspondence with the dI/dV lock-in maps is good.
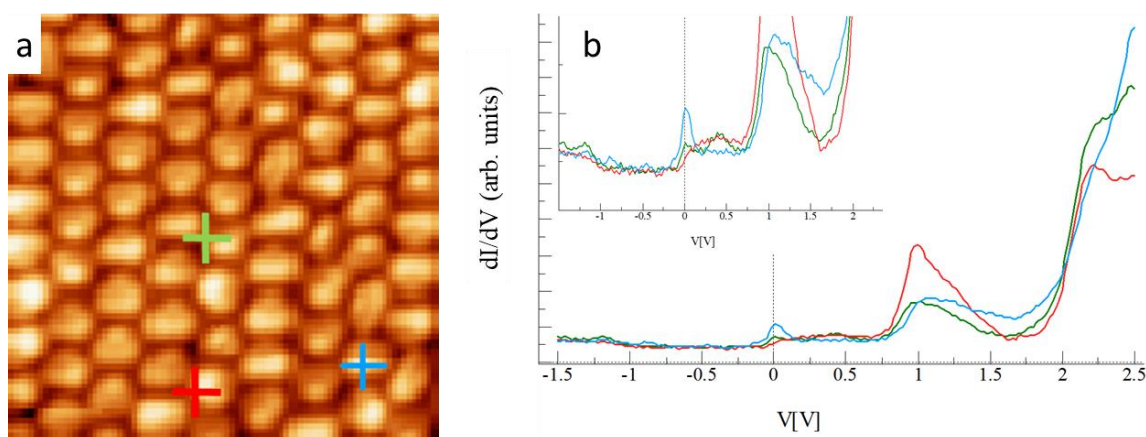

Figure 13: a) Topography image of C_{90} on Ag (111), the crosses indicate where the spectra were taken. b) dI/dV spectra taken from image a. Image information (Image size, bias voltage, tunnelling current) a) 10 x 10 nm; 2.50 V; 1.0 nA.
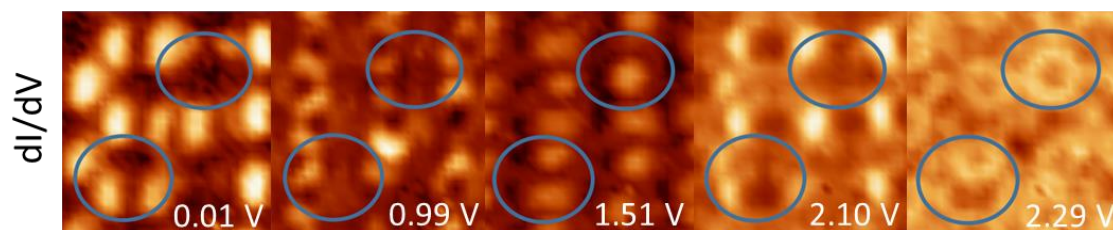
Figure 14: dI/dV images of C$_{90}$ on Ag (111) from CITS at different bias voltages. Image information (tunnelling current) 1.0 nA.

4.2. C$_{90}$/Au (111)

4.2.1. Self-assembly

The deposition of the molecules on this substrate lasted 3 hours at 480 ºC. In Figure 15a a topography image of an island of these molecules is presented. In addition, from this image we took a height profile shown in Figure 15b which indicates that the height of the islands is similar to the Van der Waals diameter of C$_{90}$. They self-assemble in a rhomboidal order as in Ag (111). In order to calculate the unit cell, we measured some relevant parameters shown in Table 2 considering the shape of the molecule ellipsoidal, as found in the STM images like in Figure 16. This image shows an intermolecular resolution topography image of the previous island (Figure 15) including the calculated parameters of the unit cell of the molecules and the high symmetry directions of the substrate.
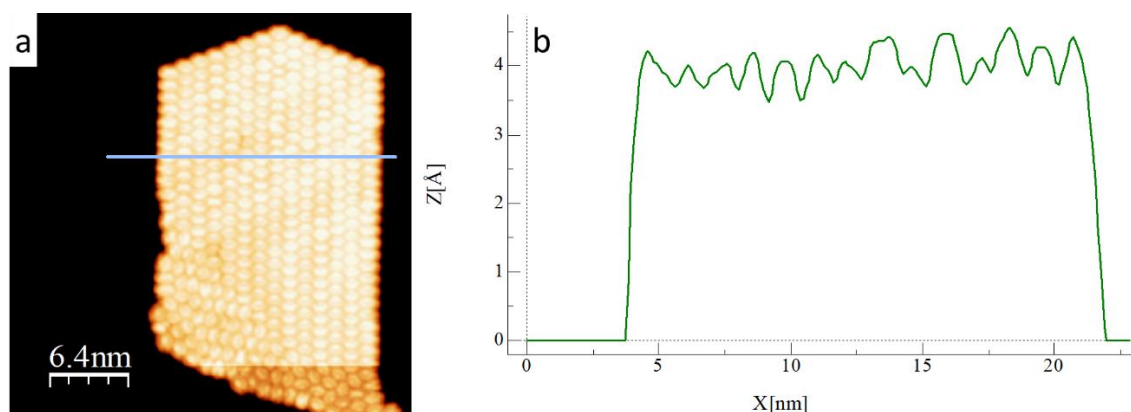

Figure 15: a) Topography image of C$_{90}$ on Au (111). b) Height profile of image a. Image information (Image size, bias voltage, tunnelling current) 32.0 x 32.0 nm; 2.00 V; 30.0 pA.
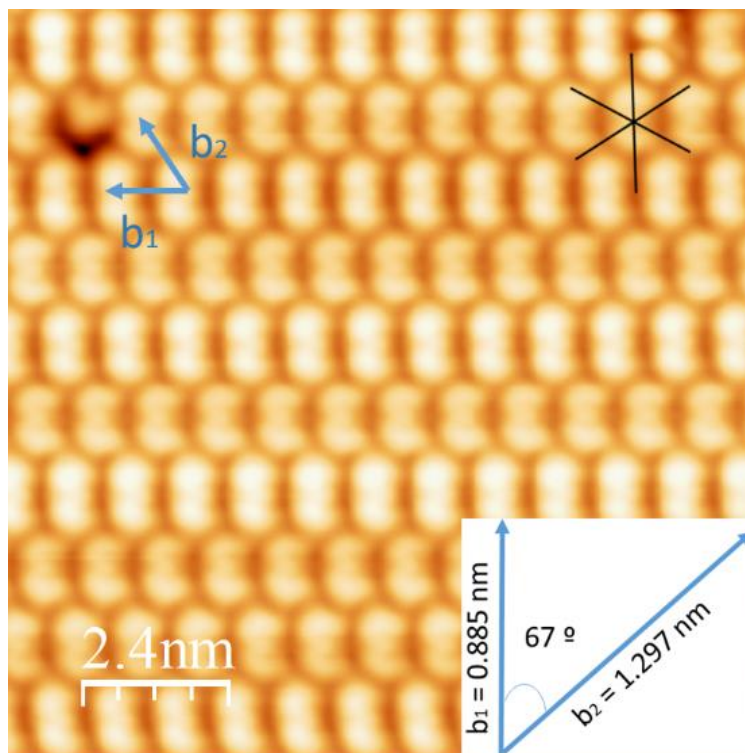
Figure 16: Intramolecular resolution image of C_{90} on Au (111). Vectors b_1 and b_2 are the lattice vectors. The black star is the high symmetry directions of the substrate. Image information (Image size, bias voltage, tunnelling current) 12.0 x 12.0 nm; 1.10 V; 500.0 pA.
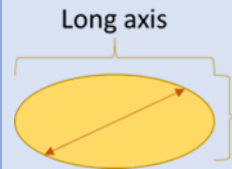
Measurement	Value (nm)			
Long axis distance	1.28 ± 0.04*			
Short axis distance	0.82 ± 0.03*			
Mean intermolecular diagonal distance (b_2)	1.297			
Mean intermolecular vertical distance (b_1)	0.885			

Table 2: Measurements of the most relevant distances of C_{90} in Au (111). *Statistical values.

As in the case of the Ag (111) substrate, we created a schematic lattice of the molecules and the substrate (Figure 17) and we observed that the interaction of the molecules with Au (111) is approximately equivalent as in Ag (111). The relation between the lattice vectors of C_{90} and Au (111) is very close to the previous one, but the match to integer numbers is not as good. This suggests that the exact position of C_{90} molecules with

respect to the Au atoms of the substrate is less important than the intermolecular interactions to dictate the molecular arrangement.
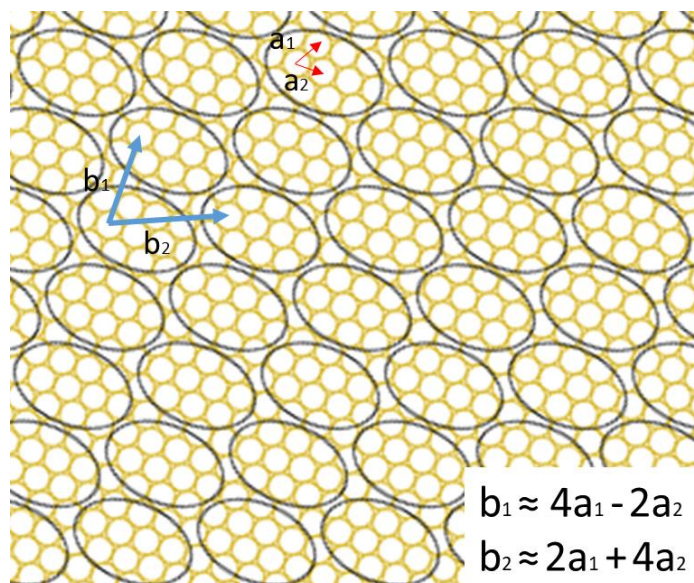

$$b_1 \approx 4a_1 - 2a_2$$
$$b_2 \approx 2a_1 + 4a_2$$

Figure 17: Schematic lattice of C_{90} on Au (111) including the relation between the lattice vectors of the molecules (b_1, b_2) and the substrate (a_1, a_2).

4.2.2. Electronic structure

From a CITS's topography image of C_{90} on Au (111) as it is shown in Figure 18a, we selected four spectra shown in Figure 18b. In this case, the HOMO level of the molecule is approximately at -1.0 V whereas the LUMO level is at 0.75 V, we found other characteristic peaks at 1.0 V and 1.75 V The spatial distribution of the dI/dV peaks has been investigated by CITS, and shown in Figure 19.
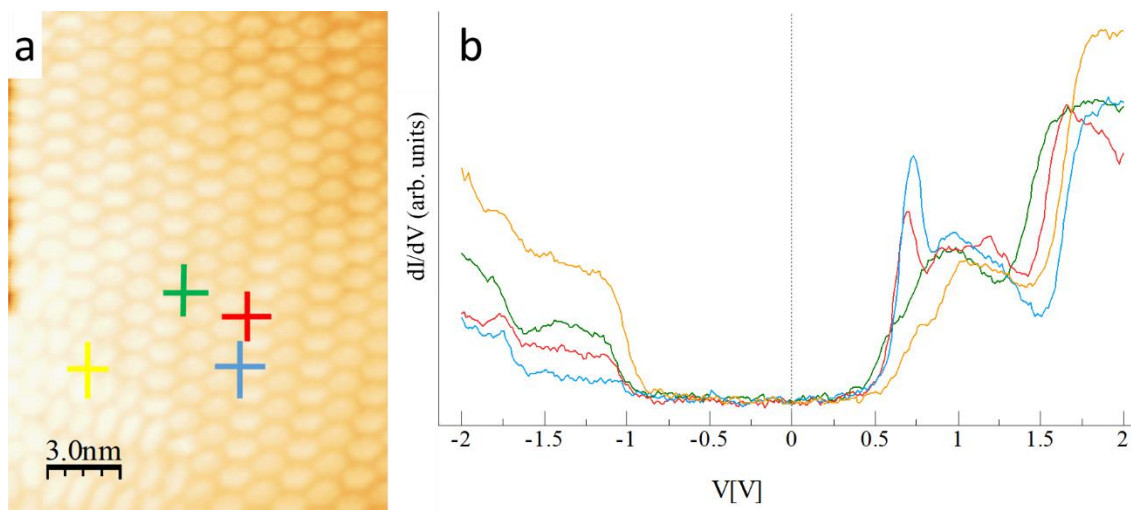

Figure 18: a) Topography image of C_{90} on Au (111), the crosses indicate where the spectra were taken. b) dI/dV spectra taken from image a. Image information (Image size, bias voltage, tunnelling current) a) 15.0 x 20.0 nm; 2.00 V; 300.0 pA.
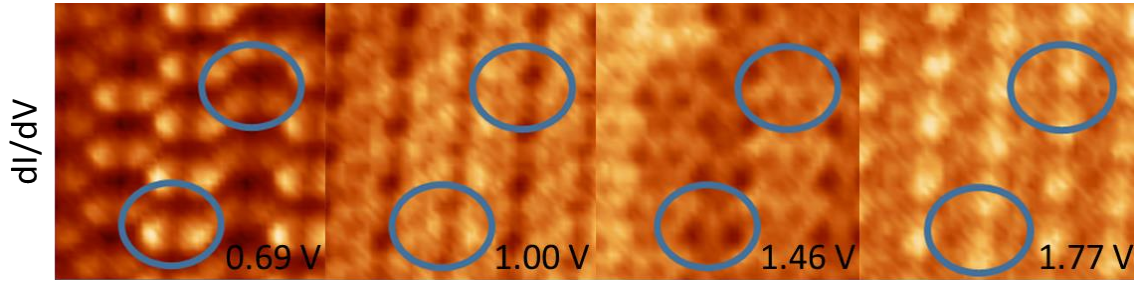
Figure 19: dI/dV images of C$_{90}$ on Ag (111) from CITS at different bias voltages. Image information (Tunnelling current) 300.0 pA.

4.3. Comparison between the electronic structure of C$_{90}$/Ag (111) and C$_{90}$/Au (111)

Comparing the dI/dV images of the two different substrates at the voltages of the characteristic peaks as it is shown in Figure 20, we observed, as we expected, the same shape of the molecular orbitals. In Figure 21, the spectra of C$_{90}$/Au (111) and C$_{90}$/Ag (111) are shown. We observe that the HOMO level appears at approximately the same energy on both substrates. However, the unoccupied peaks appear shifted by 0.6 V which is similar to the difference on the work functions of both substrates ($\phi_{Au\ (111)} = 5.31\ eV$ and $\phi_{Ag\ (111)} = 4.74\ eV$), [15] this is $\Delta E \approx 0.6\ eV$.
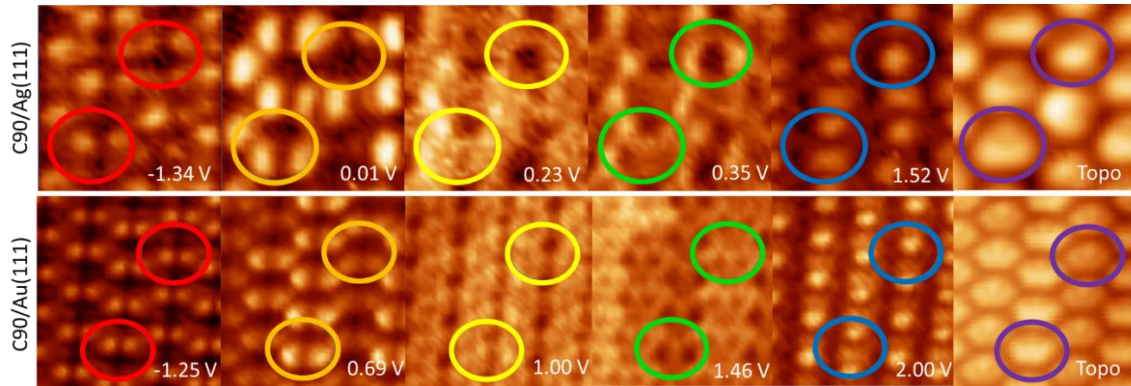

Figure 20: Relation between dI/dV images of C$_{90}$ on Ag (111) and Au (111) at different bias voltages. Image information (Tunnelling current) C$_{90}$/Ag (111) 1.0 nA, C$_{90}$/Au (111) 300.0 pA.
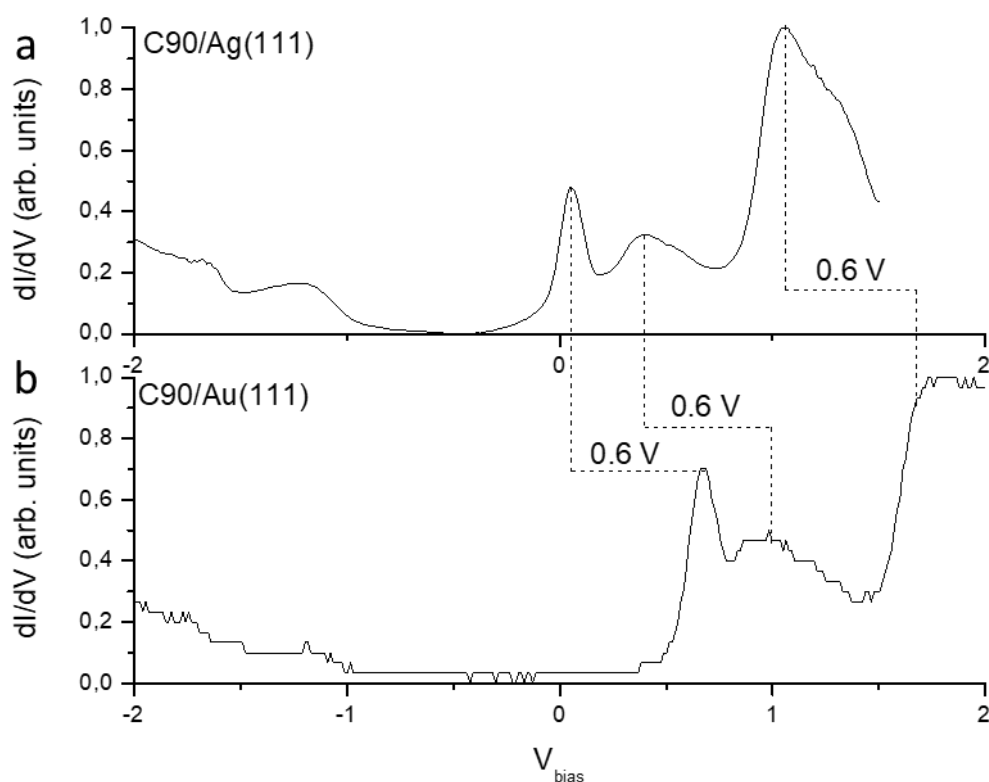
Figure 21: a) Spectrum of C_{90} on Ag (111). b) Spectrum of C_{90} on Au (111). Notice the shifted peaks at positive bias voltages.

4.4. C_{90} on NaCl on Ag (111)

4.4.1. Self-assembly

In the previous sections we have found that the assembly and electronic structure of C_{90} molecules on metal surfaces is strongly influenced by the substrate. In order to study C_{90} in similar conditions as if it were isolated, we deposited some insulator layers of NaCl between C_{90} and Ag (111). The sublimation of NaCl was at 470 ºC for 1 hour, and after thermalization, the deposition of C_{90} was done at 480 ºC for 3 hours. In Figure 22a, we observe some patches of NaCl and islands of C_{90} on top of them. The profile obtained for the terraces of NaCl shown in Figure 22d, let us identify that the darkest area corresponds to Ag (111), the step of approximately 0.306 nm, the first layer of NaCl and the next steps the successive layers of the salt.

As for the C_{90} island, we observe that the height is much larger than the measurements on Ag (111) or Au (111) reaching approximately 1.39 nm (Figure 22e). This height matches the long axis distance of the molecule. In Figure 22b, we observe a molecularly resolved region of an island which indicates that C_{90} self-assembles in a hexagonal lattice (Fourier image also indicate this, see Figure 22c). Finally, in Figure 22b we also observe

that the C_{90} molecules present a circular instead of ellipsoidal shape with a diameter similar to Van der Waals' diameter of the tube section (Table 3). Thus, we can conclude that they self-assembly in hexagonal order with its long axis perpendicular to the surface and what is being observed is the upper part of C_{90}. This way of self-assembly is similar to CNT's.
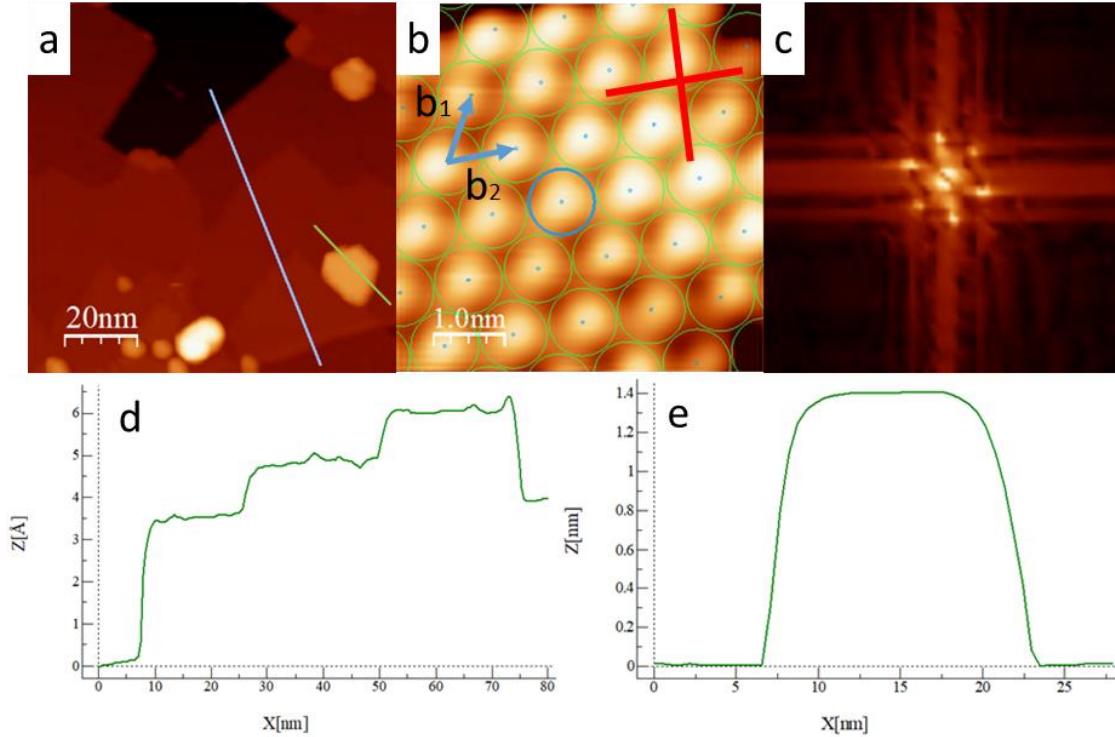

Figure 22: a) Topography image of C_{90} on NaCl covered Ag (111) b) Topography image of the surface of a C_{90} island. A schematic lattice is presented on top of the image. b_1 and b_2 are its lattice vectors and the red cross the high symmetry directions of NaCl. c) Fourier image of b. d) Height profile of NaCl. e) Height profile of C_{90} island on NaCl covered Ag (111). Image information (Image size, bias voltage, tunnelling current) a) 100.0 x 100.0 nm; 2.10 V; 30.0 pA b) 5.0 x 5.0 nm; 0.50 V; 250.0 pA.

Measurement	Value (nm)
Intermolecular distance	0.95 ± 0.05*
Diameter of the molecule	0.79 ± 0.03*

Table 3: Measurements of the intermolecular distance and diameter of the molecules. *Statistical values.

The purpose of using NaCl layers is to maximize the interaction between the molecules and minimize the interaction with the metallic substrate. Moreover, we observed that one side of the island is always parallel to another one of the patch of NaCl below it.

4.4.2. Electronic structure

The lock-in maps at different bias voltages show the changes of the shape of the orbitals, following one molecule, in Figure 23, we selected the main changes in the orbital shape. Thus, for 1.2 V the MO's shape is triangular seen in Figure 23a whereas at -0.7 V it presents two lobes shape as it is demonstrated in Figure 23b, forming a honeycomb structure. For better visualization a 3D model at -0.8 V have been created in Figure 23c. Due to its geometry, the pentagon of the molecule is placed on top and on bottom as in this substrate they are placed with its long axis perpendicular to the surface. In the case of C_{60} fullerenes, as they present spherical geometry, they do not always arrange so the pentagon is on top [16].
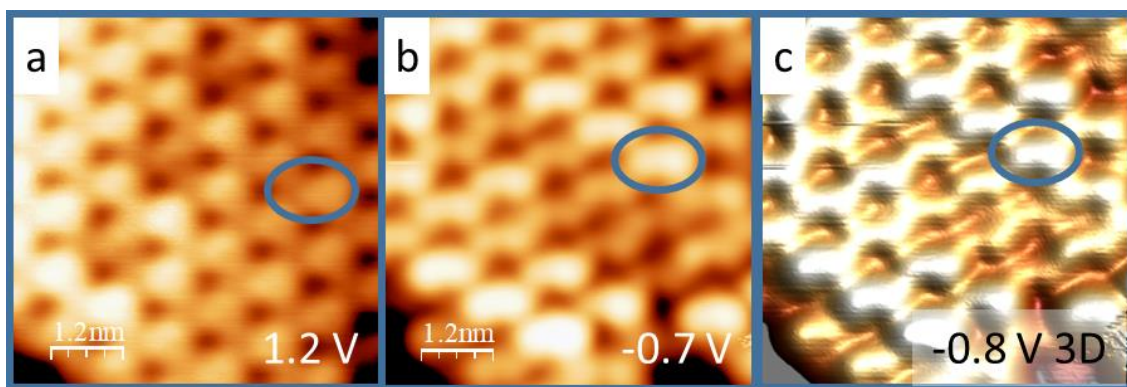

Figure 23: Topography images of C_{90}/NaCl/Ag (111) at different bias voltages. Also, a 3D model at -0.8 V is presented. Image information (Image size, tunnelling current) a) 6.0 x 6.0 nm; 600.0 pA b) 6.0 x 6.0 nm; 350.0 pA c) 6.0 x 6.0 nm; 400.0 pA.

5. Conclusions

In this Master Thesis we have studied the self-assembly and the electronic structure of the isomer $D_{5h}(I)$-C_{90} in three different surfaces. This lead us to the following conclusions. Topography images reveal that for C_{90}/Ag (111) and C_{90}/Au (111) the molecules arrange following a rhomboidal self-assembly in which the molecules are placed horizontally. The long axis is parallel to the substrate and subsequent close-packing in the molecular arrangement. Molecule-substrate interaction is stronger than molecule-molecule interaction and thus CNT-like formation of bundles is not observed.

The measurements taken have lead us to propose model lattices for C_{90}/Ag (111) and C_{90}/Au (111). For C_{90}/Ag (111), there is an integer relation between the lattice vectors of the molecules and the lattice vectors of Ag atoms. In the case of C_{90}/Au (111), the relation between the lattice vectors is not exactly integer although similar to the one

presented for C_{90}/Ag (111). To dictate the molecular arrangement, the exact position of C_{90} molecules with respect Au (111) is less important than the intermolecular interactions.

Topography images of C_{90}/NaCl/Ag (111) reveal that the arrangement is hexagonal. Fourier transform images also indicate this. The long axis of the molecules is perpendicular to the substrate, this way of self-assembly is similar to CNT's. This has to do with the way molecules electronically interact in order to minimize their energy, thus, they always interact with the maximum area possible and with the most electronic interactive material.

Regarding the electronic structure, depending on the substrate, particular shapes of this orbitals appeared at different bias voltages. After following a single molecule through all lock-in maps it was possible to determine the exact shape of the orbitals for the two noble metals and the NaCl covered Ag (111). From CITS, we could relate the shape of the orbitals seen on the lock-in maps with the spectra taken from certain parts of the molecules. These spectra showed the position of the HOMO and LUMO levels of the molecules. By comparing the spectra taken for C_{90}/Ag (111) and C_{90}/Au (111) it was observed that the HOMO levels of the molecule are not shifted whereas the LUMO level and the rest of the peaks shown in the spectra are shifted by approximately 0.6 V which is the difference between the work functions of Ag (111) and Au (111).

In general, we have found different recipes for the fabrication of C_{90} nanostructures on a variety of substrates, and their geometrical and electronic structure have been studied. Thus, by changing the interaction of the molecules with the sample we obtain fullerenes-like or CNT's-like properties. These investigations should pave the way for further work that will allow us to explore the boundaries between fullerene and nanotubes.

Acknowledgements

References

[1] A. Belkin, A. Hubler & A. Bezryadin, "Self-Assembled Wiggling Nano-Structures and the Principle of Maximum Entropy Production," *Scientific reports,* vol. 5, 2015.

[2] G. Lalwani, B. Sitharaman, "Multifunctional Fullerene-and Metallofullerene-Based Nanobiomaterials," *Nano LIFE,* vol. 3, 2013.

[3] Y. He, H. Y. Chen, J. Hou, Y. Li, "Indene−C60 bisadduct: a new acceptor for high-performance polymer solar cells," *Journal of the American Chemical Society,* vol. 132(4), pp. 1377-1382, 2010.

[4] D. Janas, A. C. Vilatela, K. K.K. Koziol, "Performance of carbon nanotube wires in extreme conditions," *Carbon,* vol. 62, pp. 438-446, 2013.

[5] "marketsandmarkets," [Online]. Available: https://www.marketsandmarkets.com/Market-Reports/carbon-nanotubes-

139.html?gclid=Cj0KCQjw6IfoBRCiARIsAF6q06sOcb1_iAPBtZ5LIMDSPW79N8xS5 rj0shgPVtwWwS67u3P01kcbG-UaAjHCEALw_wcB.

[6]   "Publications on carbon nanotube applications including scaffold microfabrication," [Online]. Available: nano.byu.edu.

[7]   C.W. Tan, K.H. Tan, Y.T. Ong, et al., "Energy and environmental applications of carbon nanotubes," *Environ Chem Lett,* vol. 10, p. 265–273, 2012.

[8]   G. Binnig, H. Rohrer, "Scanning tunneling microscopy," *IBM Journal of Research and Development,* vol. 30 (4), p. 355–69, 1986.

[9]   "The Nobel Prize," [Online]. Available: https://www.nobelprize.org/prizes/physics/1986/press-release/.

[10]   C. Cohen-Tannoudji, B. Diu, F. Laloe, "Quantum mechanics, vol. 1," *Wiley; Edition: 1st,* 8-01-1991.

[11]   "Chemistry LibreTexts," [Online]. Available: https://chem.libretexts.org/Bookshelves/Physical_and_Theoretical_Chemistry_ Textbook_Maps/Supplemental_Modules_(Physical_and_Theoretical_Chemistry) /Quantum_Mechanics/02._Fundamental_Concepts_of_Quantum_Mechanics/T unneling.

[12]   C. Bai, "Scanning tunneling microscopy and its applications," *Springer Verlag,* 2000.

[13]   C. Kittel, "Introduction To Solid State Physics 8Th Edition," *John Wiley & Sons, Inc,* 2005.

[14]   A. L. V. De Parga, R. Miranda, "Encyclopedia of nanotechnology," *Choice Reviews Online,* vol. 50 (06), pp. 50-3014, 2013.

[15]   J. Hölzl, F. K. Schulte,, "Work functions in metals, in Solid Surface Physics," *Springer-Verlag,* 1979.

[16]   A. Martín Jiménez, "Electronic and optical properties at the nanoscale studied by STM," 2018.